

## Theoretical Study of the Decomposition Reactions of 2-Vinylfuran

Wei He, Qichun Zhang, Kaixuan Chen, Yusen Nie, Yan Li, Liucun Zhu,\* and Kang Shen\*

Cite This: *ACS Omega* 2024, 9, 19063–19070

Read Online

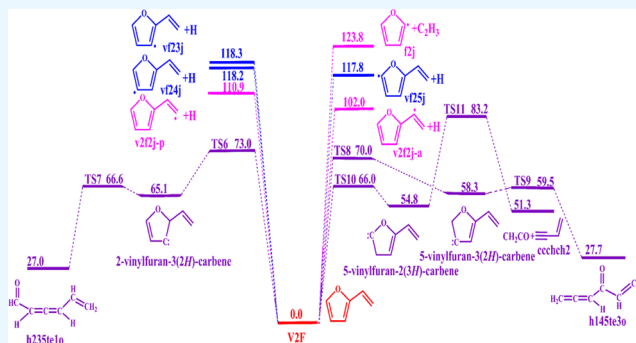
ACCESS |

Metrics &amp; More

Article Recommendations

Supporting Information

**ABSTRACT:** With the development of new synthetic methods, 2-vinylfuran (V2F) has become a potential renewable biofuel. In this work, the potential energy surfaces for the V2F unimolecular dissociation reaction, the H-addition reaction, and the H-abstraction reaction were constructed at the G4 level. The temperature- and pressure-dependent rate constants for the relevant reactions on the potential energy surfaces were calculated by solving the master equation based on the transition state theory and Rice–Ramsperger–Kassel–Marcus theory. The results show that the rate constant for the intramolecular H-transfer reaction of V2F with H atoms from the C(5) site to the C(4) site to form 2-vinylfuran-3(2H)-carbene, followed by the decomposition to form h145te3o, is the highest. The rate constants for the H-abstraction reaction of V2F with H atoms were the largest at C(6) on the branched chain, followed by C(7), and the rate constants for the H-abstraction reaction at C(3), C(4), and C(5) on the furan ring were not competitive. Negative temperature coefficient effects are observed for the rate constants of the addition reactions of V2F with H atoms at low pressures, with the H-addition rate constant at the C(5) site being the largest. This work not only provides the necessary rate constants for the reaction mechanism of V2F combustion but also provides theoretical guidance for the practical application of furan-based fuels.



## 1. INTRODUCTION

The nonrenewable nature of fossil fuels and the harmful effects of their combustion products on the environment have driven the development of biomass fuels.<sup>1–3</sup> Biomass fuels are renewable, environmentally friendly and may be used directly or as additives without changing the structure of existing internal combustion engines, and have a high potential to become an important component of sustainable energy systems in the future.<sup>4–6</sup> Furan-based biomass fuels have physicochemical properties similar to gasoline and may be used in directly existing internal combustion engines as an alternative fuel to gasoline or as an octane enhancer for gasoline.<sup>7,8</sup>

With the development of methods to convert biomass into furan-based biofuels, furan-based fuels have received increasing attention, and their combustion reaction kinetics is one of the current hot spots of research in the field of combustion.<sup>9,10</sup> Furan-based biofuels, including furan, 2-methylfuran, 3-methylfuran, 2-ethylfuran (EF2), 2,5-dimethylfuran, 2-acetyl-furan, furfural, 2-furfuryl alcohol and methyl 2-furoate, have attracted much attention.<sup>11–26</sup>

Tian et al.<sup>11</sup> carried out laminar burning velocity experiments for 2,5-dimethylfuran, gasoline, and ethanol at different initial temperatures, and the results showed that ethanol had the highest laminar burning velocity among the three fuels, followed by gasoline, and the lowest for 2,5-dimethylfuran. Tian et al.<sup>12</sup> carried out furan premixed laminar flame

experiments with different equivalence ratios at a pressure of 35 Torr and constructed a kinetic model of furan based on quantum chemical calculations. The results show that furan combustion under the current conditions hardly produces aromatic species. Sirjean et al.<sup>13</sup> developed a model for the oxidation of 2,5-dimethylfuran based on theoretical calculations and measured the ignition delay time by a stoked tube device, which showed that the model was able to predict the experimental results well. Uygun et al.<sup>14</sup> carried out high-pressure (20 and 40 bar) ignition experiments of 2-methylfuran and tetrahydrofuran in a shock tube and recorded the ignition process of 2-methylfuran and tetrahydrofuran by a high-speed camera. The results showed a two-stage ignition behavior of tetrahydrofuran at 40 bar. Eldeeb et al.<sup>15</sup> performed ignition delay time experiments with 2,5-dimethylfuran, EF2, isooctane, and a mixture of 2,5-dimethylfuran and isooctane in a shock tube. The results showed that the ignition delay time of EF2 was 6 times faster than that of 2,5-dimethylfuran, that of isooctane was faster than that of 2,5-dimethylfuran, and that the ignition delay time of a mixture of

Received: December 8, 2023

Revised: April 9, 2024

Accepted: April 11, 2024

Published: April 18, 2024



2,5-dimethylfuran and isooctane was in between. Xiao et al.<sup>16</sup> carried out combustion and emission performance experiments by blending different proportions of 2-methylfuran with diesel in a CI engine machine. The results showed that the carbon emission of the mixture of 2-methylfuran and diesel is much lower than that of pure diesel. Tran et al.<sup>17</sup> carried out experiments on the oxidation of furan, 2-methylfuran, and 2,5-dimethylfuran in a flow reactor. The results showed that all three fuels produce toxic oxygenated species such as acrolein, methyl vinyl ketone, furfural, and phenol. Yan et al.<sup>18</sup> investigated the pyrolysis experiments of methyl 2-furoate in a flow reactor and constructed a potential energy surface for the unimolecular dissociation reaction of methyl 2-furoate at the CBS-QB3 level to develop a model for the pyrolysis of methyl 2-furoate. Rate of production (ROP) analysis showed that the main pathways of methyl 2-furoate consumption include unimolecular dissociation reactions, *ipso*-substitution reactions, H-addition reactions, and H-abstraction reactions. Su et al.<sup>19</sup> investigated the flow tube pyrolysis of 3-methylfuran under varying pressure conditions using the SUVU-PIMS method, explored the isomerization effect of methylfuran fuels, and analyzed the effect of different methyl positions on pyrolysis. The results show that 2-methylfuran has a higher tendency to produce carbon soot compared to that of 3-methylfuran. Jin et al.<sup>20</sup> carried out low-temperature oxidation experiments and laminar burning velocity experiments of furfural in a jet stirred reactor (JSR) and a constant volume combustion bomb, respectively. The rate constants of dehydrogenation and hydrogenation reactions of furfural were calculated at the level of CBS-QB3, and a model for the full-scale combustion of furfural was constructed, which was able to predict the experimental results of the furfural well. Wang et al.<sup>21</sup> studied the low-temperature oxidation experiments of 2-methylfuran in a JSR. The results showed that the consumption pathways of 2-methylfuran in low-temperature oxidation were mainly OH/H atom addition and methyl H-abstraction reactions on the side chain, while the contribution of unimolecular dissociation reactions was almost negligible. He et al.<sup>22</sup> carried out pyrolysis experiments of 2-acetylfuran in a JSR by SVUV-PIMS combined with gas chromatography. In addition, the dissociation potential energy surface of 2-acetylfuran was constructed at the level of CBS-QB3 by theoretical calculations, and the rate constants of the relevant reactions on the potential energy surface were calculated by solving the master equation based on the transition state theory and the Rice–Ramsperger–Kassel–Marcus theory, as well as the Eckart tunneling effect correction. The results showed that the main consumable pathways of pyrolysis of 2-acetylfuran were the unimolecular dissociation reaction, which generated 2-furanyl + acetyl and furfuryl + methyl, and the H-addition reaction, in which the H atom was added to C(5) to generate 2,3-dihydro-5-acetyl-3-furanyl or eliminated to generate furan + acetyl. Li et al.<sup>23</sup> investigated the low-temperature oxidation of EF2 in a JSR and refined a detailed low-temperature oxidation kinetic model containing 723 species and 3300 reactions by analogy and theoretical calculations. The results show no significant negative temperature coefficient behavior for EF2, and H-abstraction and OH-addition reactions are the main consumption channels for EF2. Xing et al.<sup>24</sup> constructed a detailed potential energy surface (PES) for the reaction of 2-furfuryl alcohol with H at the CCSD(T)/CBS//M06-2X/def2-TZVP level and calculated the rate constants for the reaction on the PES using the

RRKM/ME method. The calculation results show that the total rate constant of the H-addition reaction channel is 3.3–10 times higher than that of the H-abstraction reaction channel. He et al.<sup>25</sup> constructed the PESs of 2-acetylfuran and OH at the CCSDT/CBS/M06–2x/cc-pVTZ level and solved the temperature and pressure rate constants. The results showed that the OH-addition reaction dominated at low temperatures, and the proportion gradually decreased to zero with the increase of temperature; at high temperatures, the H-abstraction reaction on the branched chain became the most dominant reaction pathway.

Recently, Song et al.<sup>26</sup> investigated the pyrolysis of EF2 in a flow reactor using synchrotron vacuum ultraviolet photoionization mass spectrometry and detected and measured more than 20 pyrolysis products, including methyl, 2-furanylmethyl, propargyl, acetylene, ethylene, propylene, vinyl ketone, 2-vinylfuran (V2F), furan/vinyl ketone, and benzene. By ROP and sensitivity analysis, V2F, 2-furanylmethyl, vinylketene, etc., were considered to be the most critical products in EF2 pyrolysis. There are no experimental and theoretical studies on the pyrolysis of 2-vinylfuran in the current report.

V2F serves as a potential biomass fuel and a key intermediate species in the pyrolysis of EF2. Therefore, the study of the combustion characteristics of V2F may provide theoretical guidance and experimental basis for the practical application of V2F in the future and may also further improve the kinetic modeling of furan-based fuels. However, few experimental and theoretical studies on the combustion characteristics of V2F have been reported so far.

In the current work, a detailed pyrolysis model of V2F was constructed by theoretical calculations, and the model was validated by EF2 pyrolysis experiments.<sup>26</sup>

## 2. METHODS

**2.1. Electronic Structure Methods.** PESs for V2F unimolecular dissociation, H-abstraction, and H-addition reactions were obtained by the G4 method,<sup>27</sup> which uses the B3LYP functional and the 6-311G(2df, p) basis set for structure optimization, frequency, and transition state calculations. All transition state structures have only one imaginary frequency. Relaxed one-dimensional scans were performed at the B3LYP/6-311G(2df, p) level at 10° increments along the dihedral angle of the corresponding species to obtain the lowest energy conformations. More precise single point energies for species on the PES were calculated at the G4 (0.1 K) level.

**2.2. Master Equation Simulations.** Based on the transition state theory and Rice–Ramsperger–Kassel–Marcus theory as well as the Eckart tunneling effect correction,<sup>28</sup> the temperature- and pressure-dependent rate constants for the reactions associated with the V2F PESs have been calculated by solving the master equations via the MESS program<sup>29,30</sup> for temperatures in the range of 200–1500 K and pressures in the range of 0.01–100 atm. The Lennard–Jones potential is used to simulate the intermolecular interactions between the target species and the bath gas (i.e., Ar). Here, the Lennard–Jones collision parameters ( $\epsilon/\text{cm}^{-1}$ ,  $\sigma/\text{Å}$ ) were estimated using the Joback group contribution method to be (325.4 and 5.50) for V2F and (79.2 and 3.47) for Ar.<sup>31</sup> The energy transfer of excited state molecules is described using a single-exponential down model. The average energy transferred in a deactivation collision is  $\langle\Delta E\rangle_{\text{down}} = 200 \times (T/200)^{0.85} \text{ cm}^{-1}$ .<sup>32</sup>

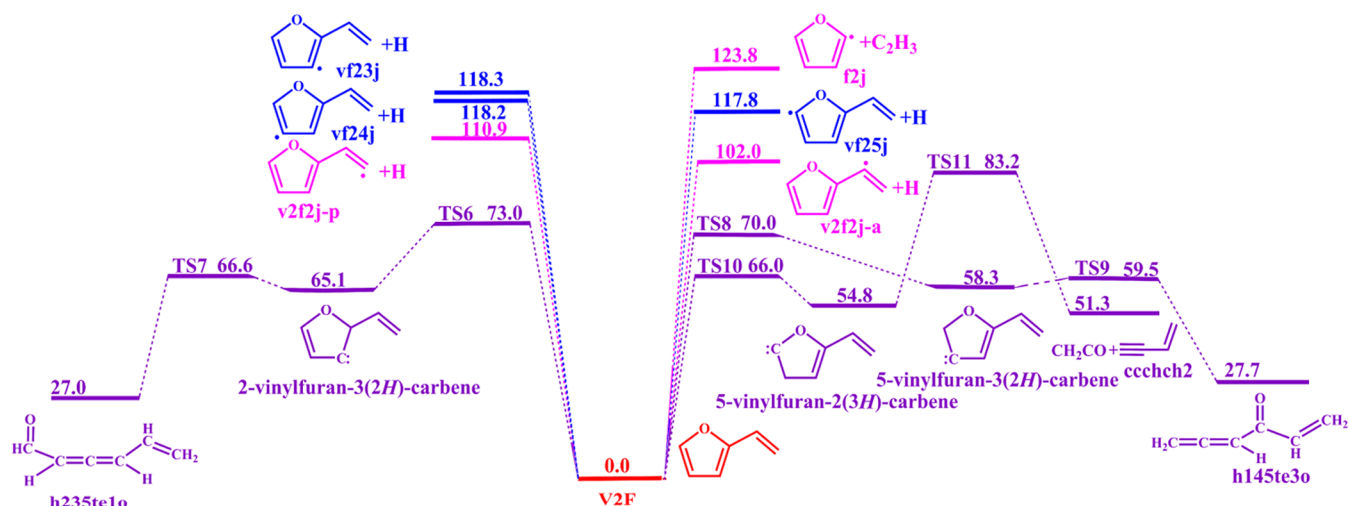


**Figure 1.** Potential energy surfaces for the main unimolecular decomposition pathways of V2F were calculated at the G4 level. The unit is in kcal·mol<sup>-1</sup>.

For unimolecular dissociation reactions without obvious transition states, the rate constants of the dissociation reactions are calculated by using the microcanonical variational transition state theory. The relaxed scan was increased from 1.5 to 4.0 Å in steps of 0.1 Å at the G4 level. Minimum energy paths were found, and frequency and single point energies were calculated.

All quantum chemical calculations were performed using the Gaussian 09 program.<sup>33</sup>

### 3. RESULT AND DISCUSSION

**3.1. Potential Energy Surfaces.** In this study, the energy scheme of G4 was used to calculate the PESs of the V2F reaction system, including unimolecular dissociation reactions, H-transfer decomposition reactions, H-abstraction reactions, and H-addition reactions.

**3.1.1. Unimolecular Dissociation Reaction Potential Energy Surface of V2F.** The unimolecular decomposition is mainly the breakage of C(7)–H, C(6)–H and C(2)–C<sub>2</sub>H<sub>3</sub> on the branched chain, forming H + 2-(furan-2-yl)vinyl radical (v2f2j-p), H + 1-(furan-2-yl)vinyl radical (v2f2j-a), and 2-furyl + vinyl (f2j + C<sub>2</sub>H<sub>3</sub>), with barriers of 110.9, 102.0, and 123.8 kcal·mol<sup>-1</sup>, respectively. Energetically, the H-dissociation channel on C(6) is more favorable than that on C(7). The C<sub>2</sub>H<sub>3</sub> dissociation reaction on C(2) requires the highest energy (Figure 1).

In addition, the current work calculates the H-dissociation reactions on the furan ring of V2F, i.e., C(3)–H, C(4)–H, and C(5), to produce the H + 2-vinylfuran-3-yl radical (v2f2j-p), H + 5-vinylfuran-3-yl radical (v2f2j-p), and H + 5-vinylfuran-3-yl radical (v2f2j-p), with energy barriers of 118.3, 118.2, and 117.8 kcal·mol<sup>-1</sup>, respectively. The V2F bond dissociation energies shown in Figure 2 also show that the H-dissociation reaction on the V2F branched chain is energetically more competitive compared with the dissociation reaction on the furan ring.

**3.1.2. H-Transfer Decomposition Potential Energy Surface of V2F.** Previous studies have found that H-transfer decomposition is one of the important consumption pathways for furan fuels.<sup>22,26</sup>

By H-transfer reaction, V2F may be converted to 2-vinylfuran-3(2H)-carbene, 5-vinylfuran-3(2H)-carbene, and 5-

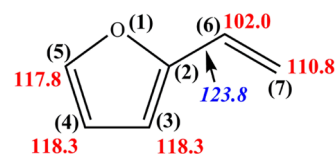


**Figure 2.** Molecular structures and bond dissociation energies (in kcal·mol<sup>-1</sup>) of V2F. Normal text, C–H bond; italic, C–C bond. Numbers in parentheses are atom labels.

vinylfuran-2(3H)-carbene, with energy barriers of 73.0 kcal·mol<sup>-1</sup> (TS6), 70.0 kcal·mol<sup>-1</sup> (TS8), and 66.0 kcal·mol<sup>-1</sup> (TS10), respectively. 2-vinylfuran-3(2H)-carbene, 5-vinylfuran-3(2H)-carbene, and 5-vinylfuran-2(3H)-carbene subsequently undergo decomposition reactions to form hexa-2,3,5-trienal (h235te1o), hexa-1,4,5-trien-3-one (h145te3o), and *but*-1-en-3-yne (ccchch2) + ketene (CH<sub>2</sub>CO) with energy barriers of 66.6 kcal·mol<sup>-1</sup> (TS7), 58.3 kcal·mol<sup>-1</sup> (TS9), and 83.2 kcal·mol<sup>-1</sup> (TS11), respectively.

From the PES it can be seen that although 5,4-H-transfer to generate 5-vinylfuran-2(3H)-carbene has the lowest energy barrier, the reaction is the most favorable, and the subsequent decomposition reaction of 5-vinylfuran-2(3H)-carbene to generate *but*-1-en-3-yne (ccchch2) + CH<sub>2</sub>CO needs to overcome a higher energy barrier, possibly resulting in this reaction channel not being competitive. Energetically, the 4,5-H-transfer reaction eventually produces h145te3o as the most competitive reaction channel.

**3.1.3. H-Abstraction Reaction Potential Energy Surface of V2F.** The PES for the H-abstraction reaction of V2F with H atoms is shown in Figure 3. The V2F side chain has two H atom abstraction sites, leading to v2f2j-a + H<sub>2</sub> and v2f2j-p + H<sub>2</sub>, with energy barriers of 12.9 kcal·mol<sup>-1</sup> (TS2) and 16.2 kcal·mol<sup>-1</sup> (TS1), respectively. The H-abstraction reaction is more likely to occur for the H atom on C(6) than for the H atom on C(7), and this is confirmed by the bond dissociation energies in Figure 2, where the dissociation energy of the H atom on C(6) is lower than that of the H atoms on C(7). There are three H atom abstraction sites on the V2F furan ring, producing V2F3j + H<sub>2</sub>, V2F4j + H<sub>2</sub>, and V2F5j + H<sub>2</sub>, which have energy barriers of 28.2, 28.6, and 21.2 kcal·mol<sup>-1</sup>, respectively. Energetically, the H atoms on the furan ring of V2F are not competitive for H-abstraction reactions.

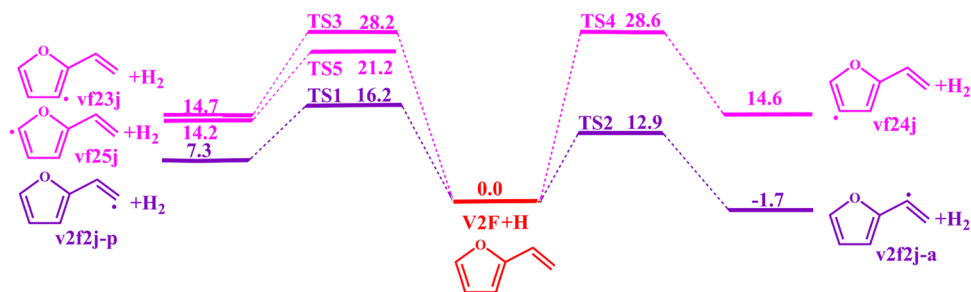


**Figure 3.** Potential energy surface for the H-abstraction reaction of V2F with H was calculated at the G4 level. The unit is in kcal·mol<sup>-1</sup>.

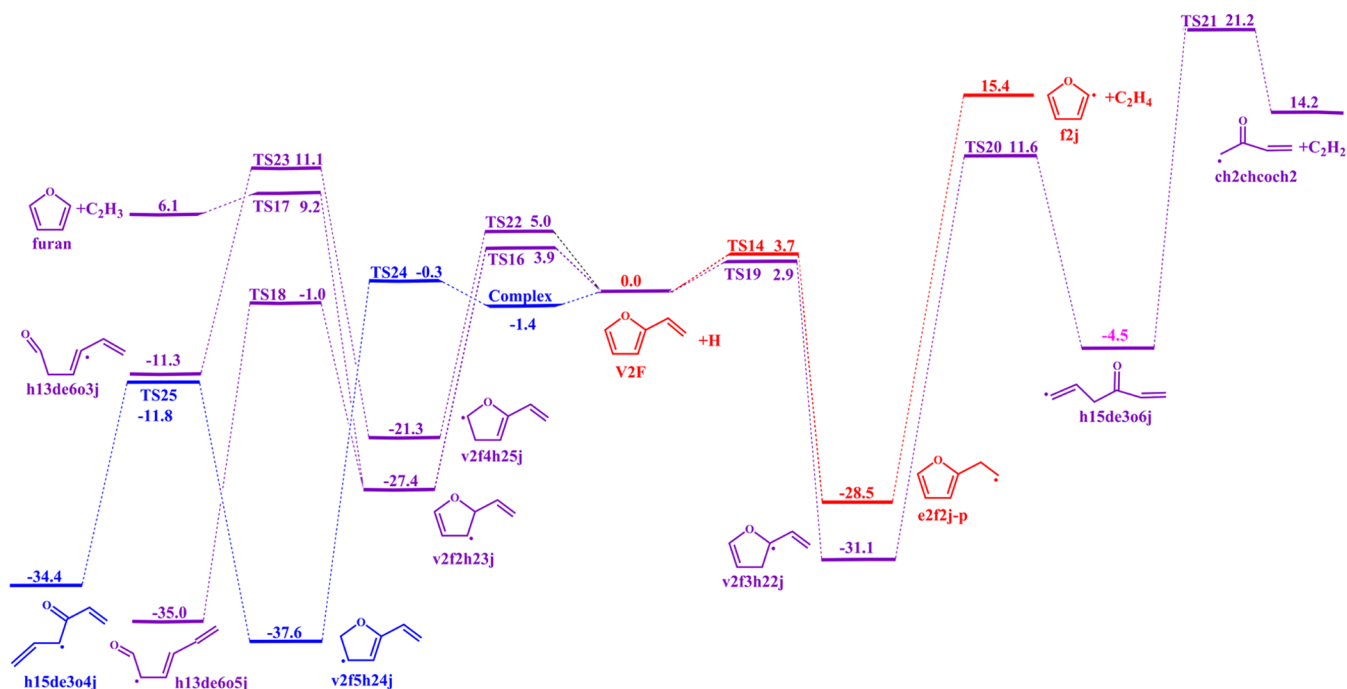


**Figure 4.** Potential energy surface for the addition reaction of V2F with H was calculated at the G4 level. The unit is in kcal·mol<sup>-1</sup>.

**3.1.4. H-Addition Reaction Potential Energy Surface of V2F.** Song et al.<sup>26</sup> studied EF2 pyrolysis experiments and found that the H-addition reaction is the main consumption pathway in the pyrolysis of V2F. Both the V2F branched chain and the furan ring have carbon–carbon double bonds (C=C), so both may lead to addition reactions. The PES for the addition reaction of V2F with H atoms is shown in Figure 4.

H-addition on the V2F ring leads to the formation of four radicals, 2-vinyl-2,3-dihydrofuran-3-yl radical (v2f2h23j), 2-vinyl-2,3-dihydrofuran-2-yl radical (v2f3h22j), 5-vinyl-2,3-dihydrofuran-3-yl radical (v2f4h25j), and 5-vinyl-2,3-dihydrofuran-2-yl radical (v2f5h24j), with energetic barriers of 3.9 kcal·mol<sup>-1</sup> (TS16), 2.9 kcal·mol<sup>-1</sup> (TS19), 5.0 kcal·mol<sup>-1</sup> (TS22), and -0.3 kcal·mol<sup>-1</sup> (TS24), respectively. V 2f2h23j is subsequently generated from (*E*)-hexa-3,5-dienal radicals (h13de6o5j) via  $\beta$ -breakage of O(1)–C(2) with an energy barrier of 26.4 kcal·mol<sup>-1</sup> (TS18). In addition, v2f2h23j could subsequently produce furan and C<sub>2</sub>H<sub>3</sub> via  $\beta$ -breaks C(2)–C(6) that have an energy barrier of 36.6 kcal·mol<sup>-1</sup> (TS17). Therefore, it is energetically more competitive for v2f2h23j to break C–O bonds compared to breaking C–C bonds. V 2f3h22j followed by a  $\beta$ -break to produce the hexa-1,5-dien-3-one radical (h15de3o4j) at the energy barrier of 42.7 kcal·mol<sup>-1</sup> (TS20). V 2f4h25j then generates (*E*)-hexa-3,5-dienal (h13de6o3j) via  $\beta$ -breaks for an energy barrier of 32.4 kcal·

mol<sup>-1</sup> (TS23). V 2f5h24j is subsequently generated via  $\beta$ -breaks to hexa-1,5-dien-3-one radical (h13de6o5j), which has an energy barrier of 25.8 kcal·mol<sup>-1</sup> (TS25).

The energy barrier of TS24 is lower than that of the initial reactants, probably due to the weak van der Waals (vdW) complexes of V2F formed with H through hydrogen bonding. The rate constants of this barrier-free reaction cannot be calculated using the conventional transition state theory; therefore, the rate constants of the process are calculated using the phase space theory.<sup>34</sup> The interaction of the reactants with the weak vdW complexes is estimated by the formula  $V(R) = C_6/R^6$ , where  $R$  is the distance between the reactants.  $C_6$  is estimated by the equation  $C_6 = \alpha_1 \alpha_2 E_1 E_2 / (E_1 + E_2)$ , where  $\alpha_i$  and  $E_i$  ( $i = 1, 2$ ) are the polarizabilities and ionization energies of the two reactants, respectively. The value of  $C_6$  in the current system is  $1.97 \times 10^8 \text{ cm}^{-1} \cdot \text{\AA}^6$  calculated from the G4 level.

**3.2. Temperature- and Pressure-Dependent Rate Coefficients.** To further clarify the effect of different reaction channels on V2F, the rate constants for the reaction on the PES were calculated by solving the master equation. Temperature ranges from 200 to 1500 K and pressure ranges from 0.01 to 100 atm were calculated for the rate constants. The rate constants for the modified Arrhenius parameters are also provided in Tables S1–S3 in the Supporting Information.

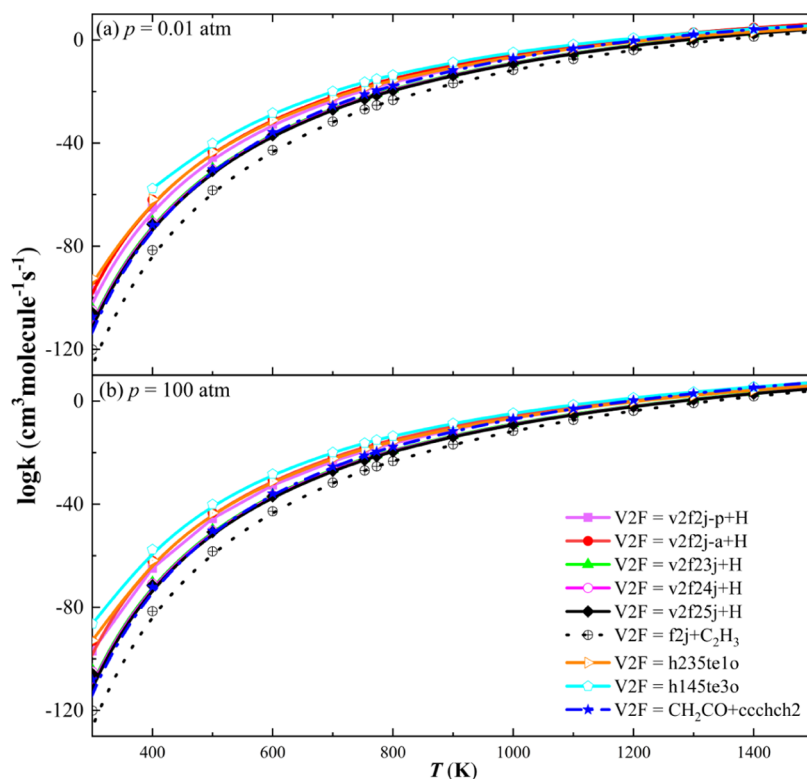


Figure 5. Rate constants for the unimolecular dissociation and intramolecular H-transfer decomposition of V2F. (a)  $p = 0.01$  atm; (b)  $p = 100$  atm.

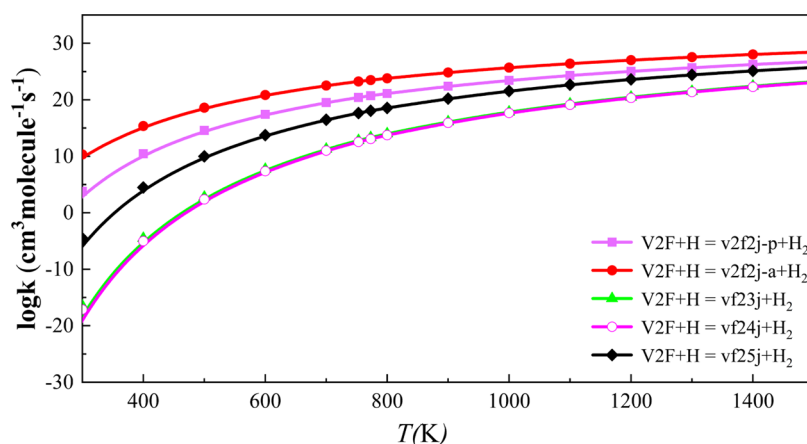


Figure 6. Rate constants for the H-abstraction reaction of V2F with H at temperatures from 300 to 1500 K.

**3.2.1. Unimolecular Dissociation and H-Transfer Decomposition Reaction Rate Constants for V2F.** The rate constants for the V2F unimolecular dissociation reaction and the intramolecular H-transfer decomposition reaction are shown in Figure 5. As can be seen, there is no negative temperature coefficient for the unimolecular dissociation reaction and intramolecular H-transfer decomposition reaction of V2F. The V2F unimolecular dissociation reaction to produce F2j + C<sub>2</sub>H<sub>3</sub> has the smallest rate constant, and the reaction channel has the highest energy barrier in the PES plot in Figure 1 also indicates that this reaction is more difficult to occur. The H-transfer from C(5) to C(4) to form 2-vinylfuran-3(2H)-carbene followed by decomposition to eventually form h145te3o has the largest rate constant. H atom dissociation at the C(6) site of the V2F branched chain to generate v2f2j-a + H and the H-transfer on C(3) to C(2) to generate 2-vinylfuran-3(2H)-

carbene followed by decomposition to ultimately generate h235te1o are also competitive with the higher rate constants of these two reaction channels. H atom dissociation reactions at the C(7) of the V2F branched chain and at the C(3), C(4), and C(5) of the furan ring have small rate constants, resulting in these reaction channels not being competitive.

From Figure 5, it can be seen that the rate constants of the H-dissociation reaction and vinyl dissociation reaction of V2F are very different at low and high pressures. The very close rate constants at low pressure may be due to the high energy barrier required for the dissociation reaction.

**3.2.2. H-Abstraction Reaction Rate Constants for V2F.** The rate constants for the H-abstraction reaction of V2F with H are listed in Figure 6. It can be seen that the H-abstraction rate constant of the H atom at the C(6) of the V2F branched chain is the largest, followed by the H atom at the C(7). H-

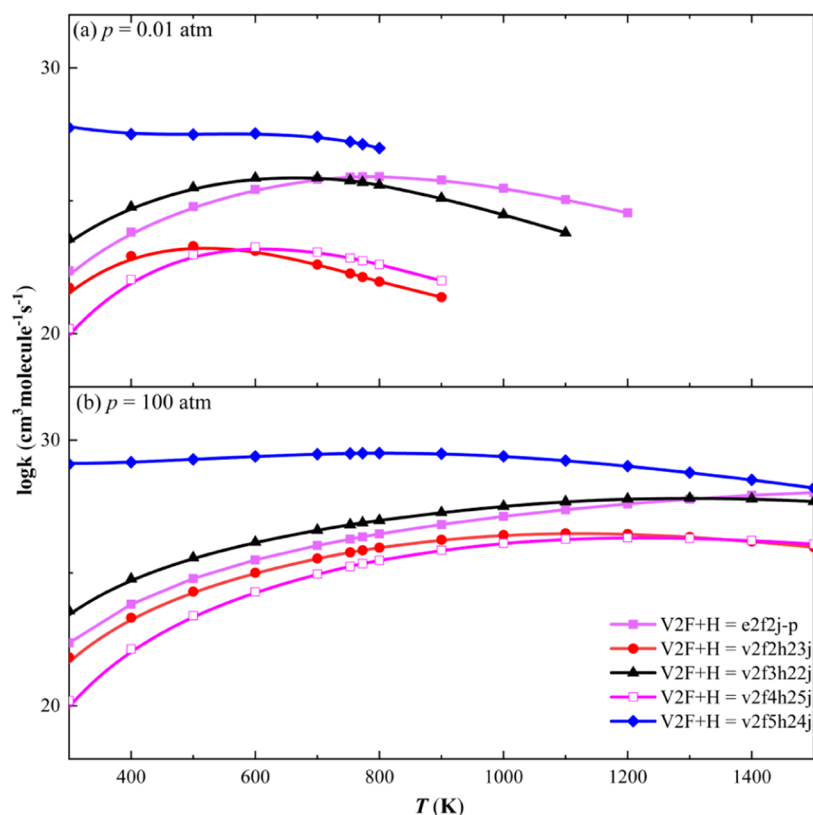


**Figure 7.** Rate constants for the addition reaction of V2F with H at temperatures from 300 to 1500 K. (a)  $p = 0.01$  atm; (b)  $p = 100$  atm.

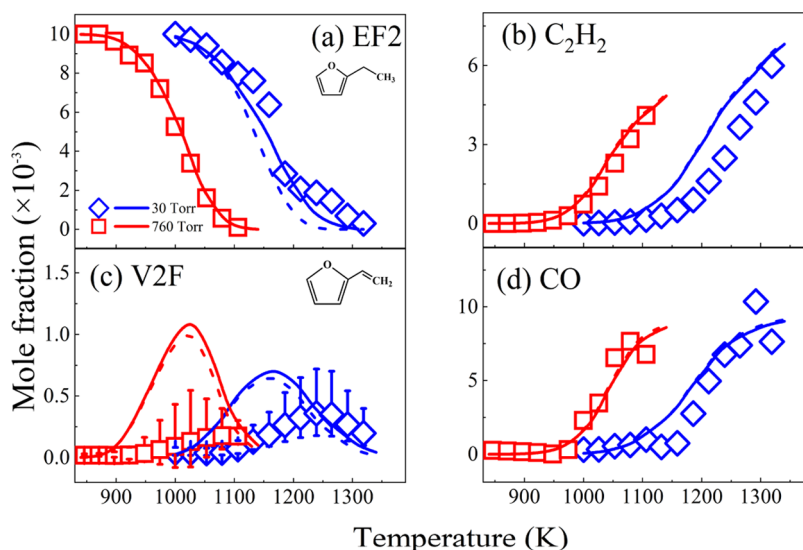


**Figure 8.** Experimental and simulated mole fraction profiles of the main species in the pyrolysis of 2-ethylfuran (EF2). (a) EF2; (b) acetylene ( $\text{C}_2\text{H}_2$ ); (c) 2-vinylfuran (V2F); and (d) carbon monoxide (CO). Symbols, solid lines, and dashed lines represent experimental data, simulation results from the updated model, and simulation results from the Song model, respectively.

abstraction rate constants for H atoms on the furan ring of V2F are much smaller than those on the branched chain, so H-abstraction reactions on the furan ring are not competitive. In addition, the rate constants for H-abstraction of H atoms at C(5) are larger than those at C(3) and C(4), which are very close to each other. This is confirmed by the bond dissociation energies of the V2F H atoms shown in Figure 2.

**3.2.4. H-Addition Reaction Rate Constants for V2F.** The rate constants for the H-addition reaction of V2F are listed in Figure 7. The H-addition reaction at the C(5) can be seen to

produce v2f5h24j with the largest rate constant as the main reaction channel. The H-addition reaction at the C(4) has the lowest rate at high pressure and is the least competitive reaction channel. In addition, the rate constant for H-addition to e2f2j-p at the C=C bond on the branched chain is also low. The H-addition reaction rate constant can be seen to decrease with increasing temperature at a pressure of 0.01 atm. The negative temperature coefficients of the rate constants for the H-addition reactions at the C(2) and C(3) sites are more

significant at low pressures, and the rate constants decrease more rapidly with increasing temperature.

#### 4. VALIDATION OF THE CALCULATED RATE COEFFICIENT

In the current work, in order to verify the accuracy of the calculated results, the calculated results were validated and compared with the experimental data and the original model. Song et al.<sup>26</sup> calculated the rate constants for the unimolecular dissociation and H-transfer decomposition reactions of EF2 at the level of CBS-QB3 and updated the pyrolysis model of Some et al. to predict the pyrolysis experiments of EF2 in a flow reactor at different pressures and temperatures. A large number of pyrolysis species were identified and measured, and in addition to common pyrolysis products such as CH<sub>4</sub>, C<sub>2</sub>H<sub>2</sub>, C<sub>2</sub>H<sub>4</sub>, and CO, V2F, which has a high mole fraction in the pyrolysis of EF2, was recognized as a key pyrolysis product. The pyrolysis experiments of EF2 in a flow reactor were simulated using the Plug Flow Reactor (PFR) code in Chemkin-Pro software.<sup>35</sup>

The experimental and simulated molar fraction profiles of the main species in the pyrolysis of EF2 are presented in Figure 8, where the symbols, solid lines, and dashed lines represent the experimental data, the simulation results of the updated model, and the simulation results of the Song model, respectively.<sup>26</sup> The updated model can be seen to predict the pyrolysis of EF2 more accurately at low pressures. Both the updated model and the model of Song et al. showed higher predictions for the experimental results of V2F, probably due to the inaccurate photoionization cross section of V2F.<sup>26</sup> It may also result from inaccurate rate constants for the reaction to generate 2-vinylfuran in the original model.

#### 5. CONCLUSIONS

In this study, the pyrolysis potential energy surface (PES) of 2-vinylfuran as a potential biomass fuel has been investigated at the G4 level, including unimolecular dissociation reactions, intermolecular H-transfer reactions, H-abstraction reactions, and H-addition reactions. Then, the rate constants of the reaction channels on the potential energy surface were calculated by solving the master equation using RRKM theory and transition state theory, the effects of temperature and pressure on the rate constants were discussed, and the current experimental results were verified by pyrolysis experiments of 2-ethylfuran. The intramolecular H-transfer decomposition reaction of V2F showed the highest rate constants for the transfer of H atoms from the C(5) site to the C(4) site to form 2-vinylfuran-3(2H)-carbene, which subsequently decomposes to form h145te3o. The rate constants for the H-abstraction reaction of V2F with H atoms were largest at C(6) on the branched chain, followed by C(7), and the rate constants for the H-abstraction reaction at C(3), C(4), and C(5) on the furan ring were not competitive, especially at the C(3) and C(4) sites. The rate constants for the H-addition reaction of V2F with H show a negative temperature coefficient effect at low pressures, with the rate constant for the H-addition reaction at C(5) being the largest. This study is expected to provide theoretical guidance on the possible implications of the practical application of furan-based fuels.

#### ■ ASSOCIATED CONTENT

##### Supporting Information

The Supporting Information is available free of charge at <https://pubs.acs.org/doi/10.1021/acsomega.3c09818>.

Rate constants for the modified Arrhenius parameters (PDF)

#### ■ AUTHOR INFORMATION

##### Corresponding Authors

**Liucun Zhu** – Advanced Science and Technology Research Institute, Beibu Gulf University, Qinzhou 535011, P. R. China; Research Institute for Integrated Science, Kanagawa University, Kanagawa 259-1293, Japan; Email: [lczhu@bbgu.edu.cn](mailto:lczhu@bbgu.edu.cn)

**Kang Shen** – Eastern Michigan Joint college of Engineering, Beibu Gulf University, Qinzhou 535011, P. R. China; Guangxi Key Laboratory of Ocean Engineering Equipment and Technology, Qinzhou 535011, P. R. China; College of Electrical Engineering, Guangxi University, Nanning, Guangxi 530004, P. R. China; [orcid.org/0009-0005-3547-2336](https://orcid.org/0009-0005-3547-2336); Email: [shenkang945@bbgu.edu.cn](mailto:shenkang945@bbgu.edu.cn)

##### Authors

**Wei He** – Eastern Michigan Joint college of Engineering, Beibu Gulf University, Qinzhou 535011, P. R. China; Guangxi Key Laboratory of Ocean Engineering Equipment and Technology, Qinzhou 535011, P. R. China; Education Department of Guangxi Zhuang Autonomous Region, Key Laboratory of Beibu Gulf Offshore Engineering Equipment and Technology (Beibu Gulf University), Qinzhou 535011, P. R. China; [orcid.org/0000-0002-3100-9724](https://orcid.org/0000-0002-3100-9724)

**Qichun Zhang** – Guangxi Key Laboratory of Ocean Engineering Equipment and Technology, Qinzhou 535011, P. R. China; Education Department of Guangxi Zhuang Autonomous Region, Key Laboratory of Beibu Gulf Offshore Engineering Equipment and Technology (Beibu Gulf University), Qinzhou 535011, P. R. China

**Kaixuan Chen** – Guangxi Key Laboratory of Ocean Engineering Equipment and Technology, Qinzhou 535011, P. R. China; Education Department of Guangxi Zhuang Autonomous Region, Key Laboratory of Beibu Gulf Offshore Engineering Equipment and Technology (Beibu Gulf University), Qinzhou 535011, P. R. China

**Yusen Nie** – Eastern Michigan Joint college of Engineering, Beibu Gulf University, Qinzhou 535011, P. R. China

**Yan Li** – Guangxi Key Laboratory of Ocean Engineering Equipment and Technology, Qinzhou 535011, P. R. China; Education Department of Guangxi Zhuang Autonomous Region, Key Laboratory of Beibu Gulf Offshore Engineering Equipment and Technology (Beibu Gulf University), Qinzhou 535011, P. R. China

Complete contact information is available at: <https://pubs.acs.org/10.1021/acsomega.3c09818>

##### Notes

The authors declare no competing financial interest.

#### ■ ACKNOWLEDGMENTS

This work was supported by the Bagui Scholars Program of Guangxi Zhuang Autonomous Region Project (No.2019A08) and the National Project of Foreign Experts (No.G2022033007L).

## REFERENCES

- (1) Ghasemi-Mobtaker, H.; Mostashari-Rad, F.; Saber, Z.; Chau, K. W.; Nabavi-Pelesaraei, A. Application of photovoltaic system to modify energy use, environmental damages and cumulative exergy demand of two irrigation systems-A case study: Barley production of Iran. *Renewable Energy* **2020**, *160*, 1316–1334.
- (2) Karnauskas, K. B.; Miller, S. L.; Schapiro, A. C. Fossil Fuel Combustion Is Driving Indoor CO<sub>2</sub> Toward Levels Harmful to Human Cognition. *GeoHealth* **2020**, *4* (5), No. e2019GH000237, DOI: 10.1029/2019GH000237.
- (3) Gholami, F.; Tomas, M.; Gholami, Z.; Vakili, M. Technologies for the nitrogen oxides reduction from flue gas: A review. *Sci. Total Environ.* **2020**, *714*, No. 136712, DOI: 10.1016/j.scitotenv.2020.136712.
- (4) Gottumukkala, L. D.; Haigh, K.; Gorgens, J. Trends and advances in conversion of lignocellulosic biomass to biobutanol: Microbes, bioprocesses and industrial viability. *Renewable Sustainable Energy Rev.* **2017**, *76*, 963–973.
- (5) Huang, H.; Gao, Y.; Chen, H. A.; Wu, Y. Y.; Wang, J. Y.; Yu, C. L.; Li, J. L.; Zou, C. W. Biomass briquette fuel, boiler types and pollutant emissions of industrial biomass boiler: A review. *Particuology* **2023**, *77*, 79–90.
- (6) Chen, C. X.; Bi, Y. X.; Huang, Y. T.; Huang, H. Z. Review on slagging evaluation methods of biomass fuel combustion. *J. Anal. Appl. Pyrolysis* **2021**, *155*, No. 105082, DOI: 10.1016/j.jaap.2021.105082.
- (7) Eldeeb, M. A.; Akih-Kumgeh, B. Recent Trends in the Production, Combustion and Modeling of Furan-Based Fuels. *Energies* **2018**, *11* (3), No. 512, DOI: 10.3390/en11030512.
- (8) Cai, C. M.; Zhang, T. Y.; Kumar, R.; Wyman, C. E. Integrated furfural production as a renewable fuel and chemical platform from lignocellulosic biomass. *J. Chem. Technol. Biotechnol.* **2014**, *89* (1), 2–10.
- (9) Román-Leshkov, Y.; Barrett, C. J.; Liu, Z. Y.; Dumesic, J. A. Production of dimethylfuran for liquid fuels from biomass-derived carbohydrates. *Nature* **2007**, *447* (7147), 982–985.
- (10) Zhao, H. B.; Holladay, J. E.; Brown, H.; Zhang, Z. C. Metal chlorides in ionic liquid solvents convert sugars to 5-hydroxymethylfurfural. *Science* **2007**, *316* (5831), 1597–1600.
- (11) Tian, G.; Daniel, R.; Li, H.; Xu, H.; Shuai, S.; Richards, P. Laminar Burning Velocities of 2,5-Dimethylfuran Compared with Ethanol and Gasoline. *Energy Fuels* **2010**, *24* (7), 3898–3905.
- (12) Tian, Z.; Yuan, T.; Fournet, R.; Glaude, P.-A.; Sirjean, B.; Battin-Leclerc, F.; Zhang, K.; Qi, F. An experimental and kinetic investigation of premixed furan/oxygen/argon flames. *Combust. Flame* **2011**, *158* (4), 756–773.
- (13) Sirjean, B.; Fournet, R.; Glaude, P.-A.; Battin-Leclerc, F.; Wang, W.; Oehlschlaeger, M. A. Shock Tube and Chemical Kinetic Modeling Study of the Oxidation of 2,5-Dimethylfuran. *J. Phys. Chem. A* **2013**, *117* (7), 1371–1392.
- (14) Uygun, Y.; Ishihara, S.; Olivier, H. A high pressure ignition delay time study of 2-methylfuran and tetrahydrofuran in shock tubes. *Combust. Flame* **2014**, *161* (10), 2519–2530.
- (15) Eldeeb, M. A.; Akih-Kumgeh, B. Investigation of 2,5-dimethyl furan and iso-octane ignition. *Combust. Flame* **2015**, *162* (6), 2454–2465.
- (16) Xiao, H.; Zeng, P.; Li, Z.; Zhao, L.; Fu, X. Combustion performance and emissions of 2-methylfuran diesel blends in a diesel engine. *Fuel* **2016**, *175*, 157–163.
- (17) Tran, L.-S.; Wang, Z.; Carstensen, H.-H.; Hemken, C.; Battin-Leclerc, F.; Kohse-Höinghaus, K. Comparative experimental and modeling study of the low- to moderate-temperature oxidation chemistry of 2,5-dimethylfuran, 2-methylfuran, and furan. *Combust. Flame* **2017**, *181*, 251–269.
- (18) Yan, B.; Wang, J.; Meng, Q.; Cheng, Z.; Wei, L.; Zhang, Y.; Cao, C.; Yang, J.; Chen, G. Experimental and Kinetic Modeling Studies of Methyl 2-Furoate Pyrolysis at Atmospheric Pressure. *Energy Fuels* **2019**, *33* (5), 4611–4620.
- (19) Su, H.; Wang, J.; Zou, J.; Xu, Q.; Yang, J.; Cheng, Z.; Wei, L. Pyrolysis at Low and Atmospheric Pressures. *Energy Fuels* **2020**, *34* (1), 981–988.
- (20) Jin, Z.-H.; Yu, D.; Liu, Y.-X.; Tian, Z.-Y.; Richter, S.; Braun-Unkhoff, M.; Naumann, C.; Yang, J.-Z. An experimental investigation of furfural oxidation and the development of a comprehensive combustion model. *Combust. Flame* **2021**, *226*, 200–210.
- (21) Wang, J. L.; He, S. R.; Wang, H.; Cheng, Z. J.; Wei, L. X.; Wang, J.; Yang, J. Z.; Yan, B. B.; Chen, G. Y. Experimental and kinetic modeling studies of the low-temperature oxidation of 2-methylfuran in a jet-stirred reactor. *Combust. Flame* **2021**, *233*, No. 111588, DOI: 10.1016/j.combustflame.2021.111588.
- (22) He, W.; Xu, Q.; Xie, C.; Yin, J.; Li, P.; Wang, Z.; Zhang, L.; Wei, L. Experimental and kinetic modeling studies of 2-acetylfuran pyrolysis at atmospheric pressure. *Combust. Flame* **2022**, *236*, No. 111824.
- (23) Li, P.; He, W.; Wang, J.; Song, S.; Wang, J.; Lv, T.; Yang, J.; Cheng, Z.; Wei, L. Experimental and kinetic modeling investigations on low-temperature oxidation of 2-ethylfuran in a jet-stirred reactor. *Combust. Flame* **2022**, *241*, No. 112098.
- (24) Xing, L.; He, Y.; Wang, J.; Lian, L.; Cheng, Z.; Wang, X.; Liu, M. The reactions of 2-furfuryl alcohol with hydrogen atom: A theoretical calculation and kinetic modeling analysis. *Combust. Flame* **2023**, *250*, No. 112627.
- (25) He, W.; Chen, K. X.; Zhu, L. C.; Shen, K. Theoretical Studies on the Reaction Kinetic of 2-Acetylfuran with Hydroxyl Radicals. *ACS Omega* **2023**, *8* (23), 21277–21284.
- (26) Song, S.; Wang, J.; He, W.; Lu, J.; Su, H.; Xu, Q.; Yang, J.; Cheng, Z.; Wei, L. Experimental and kinetic modeling studies of 2-ethylfuran pyrolysis at low and atmospheric pressures. *Combust. Flame* **2021**, *226*, 430–444.
- (27) Curtiss, L. A.; Redfern, P. C.; Raghavachari, K. Gaussian-4 theory. *J. Chem. Phys.* **2007**, *126* (8), No. 084108, DOI: 10.1063/1.2436888.
- (28) Eckart, C. The penetration of a potential barrier by electrons. *Phys. Rev.* **1930**, *35* (11), No. 1303, DOI: 10.1103/PhysRev.35.1303.
- (29) Georgievskii, S. J. K. Y. MESS, 2016.
- (30) Georgievskii, Y.; Miller, J. A.; Burke, M. P.; Klippenstein, S. J. Reformulation and solution of the master equation for multiple-well chemical reactions. *J. Phys. Chem. A* **2013**, *117*, 12146–12154.
- (31) Poling, B. E.; Prausnitz, J. M.; O'Connell, J. P. *The Properties of Gases and Liquids*, 5th ed.; McGraw-Hill, Inc: New York, 2001.
- (32) Klippenstein, S. J. From theoretical reaction dynamics to chemical modeling of combustion. *Proc. Combust. Inst.* **2017**, *36* (1), 77–111.
- (33) Frisch, M. J.; Trucks, G. W.; Schlegel, H. B.; Scuseria, G. E.; Robb, M. A.; Cheeseman, J. R.; Scalmani, G.; Barone, V.; Mennucci, B.; Petersson, G. A.; Nakatsuji, H.; Caricato, M.; Li, X.; Hratchian, H. P.; Izmaylov, A. F.; Bloino, J.; Zheng, G.; Sonnenberg, J. L.; Hada, M.; Ehara, M.; Toyota, K.; Fukuda, R.; Hasegawa, J.; Ishida, M.; Nakajima, T.; Honda, Y.; Kitao, O.; Nakai, H.; Vreven, T.; Montgomery, J. A., Jr.; Peralta, J. E.; Ogliaro, F.; Bearpark, M.; Heyd, J. J.; Brothers, E.; Kudin, K. N.; Staroverov, V. N.; Keith, T.; Kobayashi, R.; Normand, J.; Raghavachari, K.; Rendell, A.; Burant, J. C.; Iyengar, S. S.; Tomasi, J.; Cossi, M.; Rega, N.; Millam, J. M.; Klene, M.; Knox, J. E.; Cross, J. B.; Bakken, V. *Gaussian 09*; Gaussian, Inc.: Wallingford CT, 2013.
- (34) He, W.; Chen, K.; Zhu, L.; Shen, K. Theoretical Studies on the Reaction Kinetic of 2-Acetylfuran with Hydroxyl Radicals. *ACS Omega* **2023**, *8* (23), 21277–21284.
- (35) Chemkin-Pro 15092 Reaction Design, S. D. 2009.